Failure and Mechanical Properties of Glassy Diblock Copolymer Thin Films

Tianren Zhang,[†] Ning Wang, [‡] Robert A. Riggleman[*, †]

†Department of Chemical and Biomolecular Engineering, University of Pennsylvania, Philadelphia, Pennsylvania 19104, United States

‡ Department of Chemical and Biomolecular Engineering, University of Notre Dame, Notre Dame, Indiana 46556, United States

Abstract

Block copolymer self-assembly is affected by nanoscale confinement, which has long been known to affect interchain entanglements and dynamics of polymers. While most previous work on confined polymer glasses has focused on the properties of homopolymers, the mechanical response of glassy block copolymer thin films is still relatively unexplored. By uniaxially deforming glassy lamellar diblock copolymer films with different morphologies via molecular dynamic (MD) simulations, we demonstrate that the toughness of the films with fingerprint morphologies is higher compared to homopolymers and oriented lamellar films due to the increase in the randomness of domain orientations and entanglements. We show that the thickness impact on the mechanical properties of the block copolymers is not as big as that of the homopolymer systems. In the strain localization analysis of the block copolymer films, there are the plastic rearrangements initially clustered at the boundary between the two phases of the lamellae until close to failure, when the plasticity transitions to the center of a domain. In the block copolymer systems, crazes in the thinnest films exhibit distinct behaviors compared to

thicker films. Our studies of the film mechanics provide molecular insight into how segmental mobility and entanglements interplay with position and morphology to control the mechanics of thin polymer films.

1. Introduction

The physical properties of glassy polymer films have long been known to change drastically under nanoscale confinement.[1,2] Depending on the property measured, these changes are often attributed to increased average molecular mobility near a free surface and reduction in entanglement density, and both are known to alter mechanical behavior. Moreover, as the films thickness approaches molecular dimensions, changes in the polymer physical properties lead to changes in the failure strength. Understanding the impact of these changes on polymer film mechanics helps guide the development of new polymer materials for strong, multifunctional films.

The knowledge of mechanical property/structure relationships in ultra-thin films of polymers, where the thickness of the film is comparable to or less than the characteristic size of the molecules, has been advanced recently both by newly developed experimental techniques that directly measure the mechanical properties and predictions from simulations[3,4,13,5–12]. Ruoff and coworkers were able to use camphor to transfer centimeter-scale ultrathin films onto custom designed substrates for mechanical (tensile) testing of polycarbonate films as thin as 100nm.[14] Recently, Crosby and coworkers overcome thickness limitations by using a newly developed experimental method that allows measurement of the complete uniaxial stress-strain response of ultrathin polymer films as thin as 30 nm[4,5,15]. Their work showed that the failure stress for polystyrene (PS) at room temperature decreases for films below a threshold thickness, near R_{ee}, and observed a thickness-controlled transition in failure mode from crazing in thicker films to shear deformation zones (SDZ) in the thinnest films[4]. In our recent study, through a comparison

between molecular dynamics (MD) simulations with the uniaxial extension experiments on the polydisperse polymer thin films, the role of effective entanglements in the determination of the mechanical properties is explored and an exponential relationship between effective entanglements and the strength of the films is derived.[16]

Moving beyond homopolymers, studies have been also conducted on block copolymers to develop optimized, multifunctional materials that combine preferred properties typically disparate in homopolymer materials. Due to the nature of block copolymers that can self-assemble into well-ordered nanostructures, the inter-chain entanglements and mobility of polymers are altered within those domains, which can in turn affect the mechanical properties of the films. Although several studies on relationships between mechanical properties and block copolymer architecture and morphology have been conducted, limitations on sample dimensions and difficulty in controlling phase orientation in bulk samples have limited advances in understanding how block copolymer domain structure and mechanical properties relate, especially beyond continuum level relationships. Many previous studies have focused on rubber-glassy systems[17–21], which can exhibit enhanced toughness and the emergence of buckling phenomena. Fujimura et al.[22,23] studied the deformation of an unoriented lamellar structure of a polystyrene-polybutadiene-polystyrene (PS-b-PB-b-PS) triblock copolymer, where they demonstrated a formation of chevron-like morphology after the yield point and a disordered morphology of fragmented polystyrene dispersing in the polybutadiene matrix at very high strains. For oriented lamellar PS-b-PB-b-PS triblock copolymer films, Thomas and coworkers deformed the samples from three different loading directions (parallel, perpendicular and diagonal) relative to the lamellae structure, finding different deformation mechanisms from neck formation to a "Chevron" morphology.[24] Through MD simulation, Makke et al. demonstrated that the buckling instability results from

the competition between the growth rate of linearly unstable modes with the rate of deformation.[25,26]

For block copolymers that have only glassy domains, the details of interchain entanglements and local segmental mobility play an important role in the mechanical response; however, controlled experiments isolating these molecular effects have been limited. Lee et al. investigated the crazing process in ordered polystyrene-b-poly(2-vinylpyridine) (PS-b-P2VP) lamellar layers parallel to the substrate and observed a lower craze growth rate compared to the homopolymer and a higher ratio of craze depth to film thickness in the micronecking process.[27] Furthermore, Ryu et al. provides some insights on the influence of the chain architecture on the craze growth poly(vinylcyclohexane)-poly(ethylene) (PCHE-PE) block copolymer thin films.[28] On the simulation level, numerous SCFT studies have mapped the phase diagrams of confined block copolymers with a variety of wetting conditions, though these calculations often assume rigid boundaries that will not be present in films with a free interface.[29–33] In addition, microphase separation plays a role in altering the distribution of entanglements, particularly in the strong segregation where the average entanglement spacing of the polymers tends to decrease.[34] However, the influence of molecular mobility, entanglement and morphology on the mechanical response of ultrathin glassy-glassy block copolymer thin films from both experiments and simulations has not yet been fully explored.

In this study, we employ MD simulations to quantify and understand the mechanical response of free-standing symmetric block copolymer films, where the domains have similar glass transition temperatures, T_g. We discuss the role of morphology orientation, entanglement distributions, local dynamics, and films thickness on the mechanical response, and these quantities are then compared against those of the homopolymers. Characterizing the stress-strain relationship

in ultra-thin films, where the block copolymer structure can be explicitly controlled and characterized, provides new opportunities for understanding how these structures can provide multifunctionality, especially with regards to enhanced strength.

2 Simulation Setup

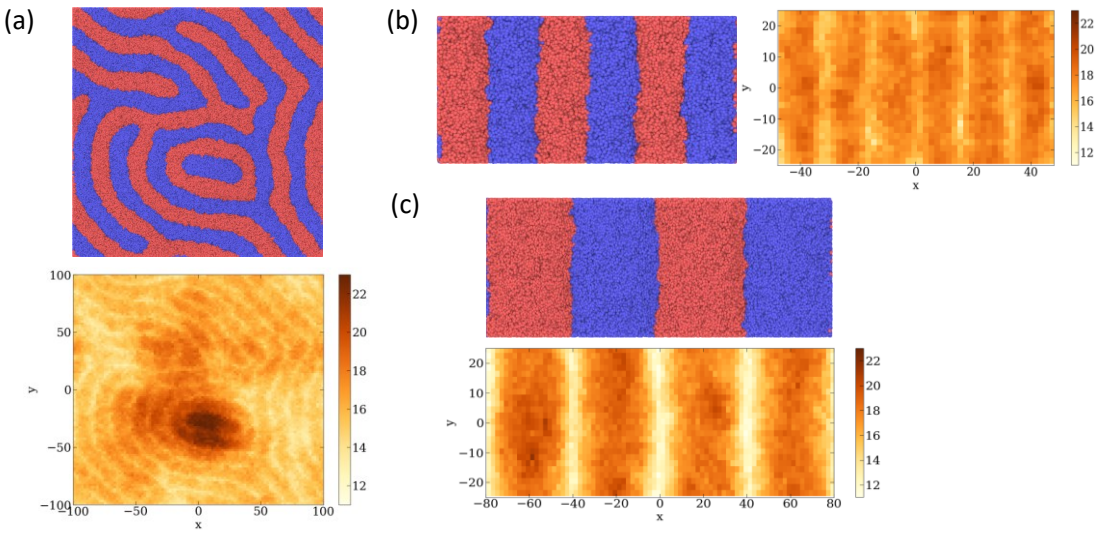

Figure 1. Film thickness heatmaps with thickness H = 20 for different chain lengths N = 60(a: fingerprint morphology) (b: ordered lamella) and N = 250 (c: ordered lamella).

Our molecular dynamics simulations employed a modified version of the bead−spring Kremer−Grest (KG) model[35], where non-bonded monomers interact through the Lennard-Jones (LJ) potential:

$$u_{nb}(r) = 4\varepsilon\left[\left(\frac{\sigma}{r}\right)^{12} - \left(\frac{\sigma}{r}\right)^{6}\right] - 4\varepsilon\left[\left(\frac{\sigma}{r_{cut}}\right)^{12} - \left(\frac{\sigma}{r_{cut}}\right)^{6}\right] \quad (6.1)$$

for $r \leq r_{cut}=2.5\sigma$. All the units are made dimensionless using the potential strength, ε, the monomer size, σ, and the unit time $\tau = \sigma\left(\frac{m}{\varepsilon}\right)^{\frac{1}{2}}$, where m is the monomer mass. The bonded interactions connecting two successive monomers are governed by a finitely extensible nonlinear elastic (FENE) potential with $k = \frac{30\varepsilon}{\sigma^2}$ and $R_0=1.5\sigma$. This bond type does not allow bond breaking during

the uniaxial deformation process. We also add an angular harmonic potential of the form $U_{ang} = \frac{K_\theta}{2}(\theta - \theta_0)^2$ where K_θ = 10/radian^2 is the strength of this interaction and $\theta_0 = 120^o$ is the equilibrium bond angle.[36] The angular potential is introduced to increase the average number of entanglements per chain without requiring very long polymer chain lengths, and the resulting average number of monomers between the entanglements is $\langle N_e \rangle \approx 16$. In this model, $T_g \approx 0.6$ as identified by monitoring the density during a simulation that cools the sample from high to low temperatures and identifying the temperature where the thermal expansion changes. The number of monomers per chain in our simulations for symmetric diblock copolymers are N = 60 or 250, with N/N_e = 3.75 and 15.1, $R_{ee} \approx 15.5 \; and \; 36.6$, respectively. Here, R_{ee} is calculated in bulk systems of diblock copolymers with oriented lamellar morphology. The interactions between pairs of A or pairs of B nonbonded monomers are set to be $\varepsilon_{AA/BB}$=1.0, and the cross interactions are set to ε_{AB}=0.7, which leads to strong microphase separation.

Films with oriented lamellar and fingerprint morphologies are constructed as shown in Figure 1. To determine the size of domain spacing of oriented lamellar films, we start with the bulk systems. For N = 60 systems, we first constructed an anisotropic simulation box with dimensions $35\sigma \times 35\sigma \times 100\sigma$ using periodic boundaries on all the directions and we assume an initial domain spacing $D \approx 2R_{ee}$, which is subsequently equilibrated as described below. The polymers are grown as biased random walks from their A-B junctions, which are initially placed at the domain centers. The biases are such that the A and B blocks are biased towards their respective domains. After constructing the systems, we introduced soft potential to gradually push the overlapping particles away from each other, and then we perform MD in the NPT ensemble with pressure $P = 0 \; \varepsilon\sigma^{-3}$ on all the dimensions to equilibrate the systems along with connectivity-altering Monte Carlo moves[37–39] for 2000τ to achieve proper domain spacing around

32σ for N = 60 and 80σ for N = 250. After equilibration, we verify that the surface tension is zero via $\gamma = \frac{L_z}{2n_p} < P_{xx} - \frac{1}{2}(P_{yy} + P_{zz}) >$ with this domain spacing in the NVT ensemble, where L_z is the box length normal to the lamella and n_p is the number of lamellar periods. Once the equilibrium domain spacing is known, it is applied in the construction of free-standing thin films following the same procedures as the bulk systems with free surfaces in z directions. After the soft push-off step, NVT ensemble along with connectivity-altering Monte Carlo moves[39,40] are applied for the equilibration process. The simulation box size for thin films in the z direction is twice the film thickness (H), and periodic boundary conditions were maintained in the plane of the film (x and y-directions).

To generate the fingerprint morphologies, the diblock polymers are randomly grown in a large simulation box with dimensions of $200\sigma \times 200\sigma \times H$ first with reflective wall on the top of the box and an amorphous substrate wall beneath them, which is meant to mimic an experimental film immediately after spin coating onto a substrate, and Dissipative particle dynamics (DPD) simulation method using soft non-bonded interactions plus bond swap is implemented to accelerate the equilibration process for 40000τ until the fingerprint structure remains stable. After the DPD simulations, we removed the reflective wall on the top to create a free surface and switched back to the NVT ensemble with the full Lennard-Jones potential for 10000τ for the production run. Due to the limitation of the simulation size, we only simulate fingerprint system with N = 60.

All the systems were equilibrated at high temperatures and were cooled down from $T = 1.0 \left(\frac{T}{T_g} = 1.67\right)$ to $T = 0.4 \left(\frac{T}{T_g} = 0.67\right)$ at a cooling rate of ΔT/Δt = 0.1 per 2000τ to the glassy state. Subsequently, we deformed each film under a constant temperature at a constant true tensile strain rate $\dot{\varepsilon} = 1 \times 10^{-4}$ in the x direction while the length in the y-dimension was

held constant and the z-dimension remained open to a free surface. While in laboratory units our deformation rate is significantly higher than experimental rates, in both experiments and simulations the rates are much faster than the equilibration time of the polymer, which gives rise to the glassy mechanical response.[4–6,16] In the systems of fingerprint morphologies, we removed the substrate before the deformation process. The film thicknesses for the oriented lamellar films are initially 10, 20 and 30σ, while for the fingerprint morphology the thickness is fixed at 20σ. In the melt states the density of the systems is approximately $\rho = 0.85\sigma^{-3}$. All the simulations are performed with LAMMPS MD simulation package.[41,42] For all the homopolymer and oriented lamellar films, three uncorrelated initial configurations were used to obtain the averaged simulation results. However, due to the large size of the system, we only performed one simulation for the fingerprint morphology.

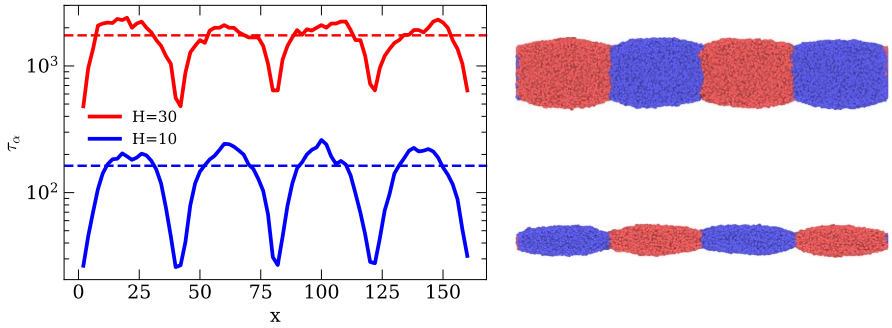

Figure 2. The relaxation time τ_α based on the particle locations along the x direction from the oriented lamellar films with N=250 at two selected film thickness. The side views of the film are provided on the right with different thickness H = 10 (bottom) and H = 30 (top). Dash line is the τ_α for homopolymer films at the same conditions.

3 Analysis and discussion

3.1 Film Dynamics and Entanglement Analysis

Unlike homopolymer thin films, block copolymer thin films exhibit variations in film thickness due to the competition between the interfacial tension at the free surfaces and that

between the A-B domains. To investigate the local structures of both oriented and fingerprint lamellar films, the thickness profiles are calculated from glassy films at T=0.4 as shown in Figure 1. As expected, a strong thickness perturbation is observed for both systems due to the existing of the domain boundary, where the film contracts to minimize A-B contacts. The range of thicknesses observed in the systems of N = 60 is approximately 10σ. These variations are even stronger for the long polymer chain (N = 250) than that of short chain systems (N = 60). Unlike oriented lamellar films, in the larger fingerprint simulations we also observe a long-wavelength fluctuation in the film thickness that is not confined to the A/B boundaries, as seen in the thickness projection plot in Figure 1a. This nonuniform thickness distribution across the films is also frequently observed in experiment from AFM images. Due to the domain boundaries and the perturbation in the film thickness, dynamics, entanglement distributions and the response to load of block copolymer thin films will be altered, and changes in those properties are what we investigate in this study.

To understand the segmental dynamics of the particles across the block copolymer thin films, we analyze the local α relaxation time τ_α, which is calculated using the intermediate scattering function F_s(Q, t) with Q=7.1σ^{-1}. $F_s(Q,t)$ approximately measures the characteristic time for a particle to move a distance of $\sim Q^{-1}$, and we extract τ_α by fitting $F_s(Q,t)$ with the empirical stretched exponential $exp\left(-\left[\frac{t}{\tau_\alpha}\right]^\beta\right)$, where β is the a stretching parameter between 0 and 1. We perform this calculation in the super cooled liquid regime $\left(\frac{T}{T_g}=1.05\right)$ for the oriented lamellar films with N=250 based on the z-positions of the monomers. We find that there is a large reduction in τ_α near the domain boundaries where the thickness is reduced, bringing more monomers to the proximity of the surface. The repulsive interactions that the segments experience

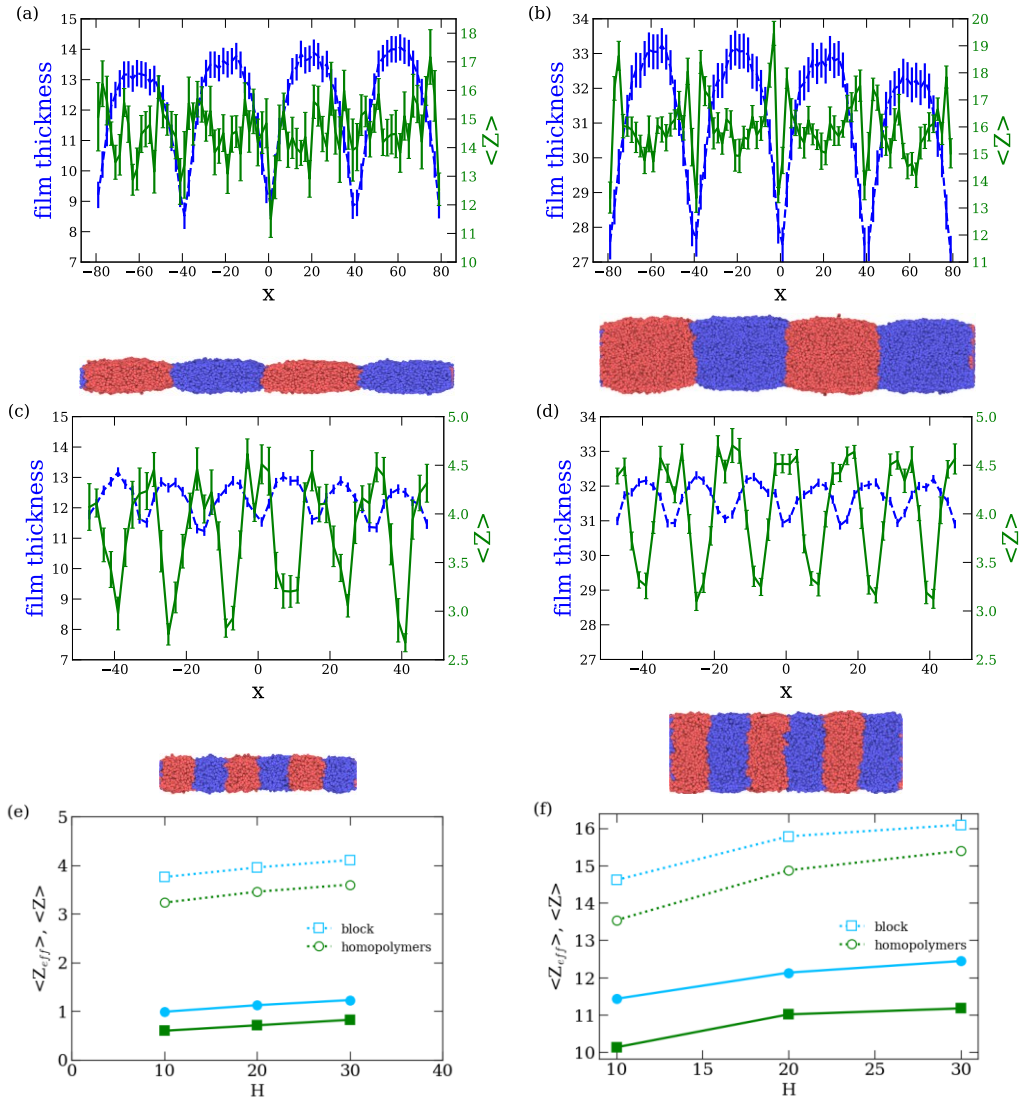

Figure 3. The film thickness profiles along the direction perpendicular to the lamella (x direction) (blue dash line) and average entanglements per chain < Z > as a function of the chain locations (green solid line) in the orientated lamellar films at two selected film thickness H =10σ (a: N = 250 and c: N=60) and H =30σ (b: N = 250 and d: N=60). The overall average entanglements per chain (dash line) and effective entanglements per chain (solid line) in the systems as function of the film thickness for N = 60 (e) and N=250 (f). Effective entanglements were defined as those where none of the primitive path steps involved in the formation of the entanglement were path steps associated with a chain end.[16] All the error bars here are standard error.

at the AB interface could be another factor that results in the reduction of τ_α near the domain boundaries.[43,44] The relaxation time in the domain centers is close to that of the homopolymer systems as shown in Figure 2. In addition to the dynamic properties, an inhomogeneous distribution of entanglements arises from the segregated morphology of the block copolymers. The entanglements per chain $\langle Z \rangle$, which is calculated from the Z1 algorithm developed by Kröger,[45,46] as a function of positions x (along the direction perpendicular to the lamella) in the oriented lamellar films in the melts at $T = 1.0$ and the average entanglements per chain of the whole systems as a function of the film thickness are shown in Figure 3. For the <Z> profile calculation, 20 independent configurations during the production run are sampled. To be consistent with <Z> profile calculation, the films thickness profile is also calculated at $T = 1.0$ using the same 20 independent configurations. Here, the thickness is calculated as the distance between the highest particle and the lowest particle along the z direction at each position on the direction perpendicular to the lamella domain. Unlike the reduction in the film thickness at the boundaries, we notice that $\langle Z \rangle$ increases near the domain boundaries, which agrees with results found in previous entanglement study and rheology study for block copolymers[34,47,48]. However, we observe a drop in $\langle Z \rangle$ at the very center of the domain boundaries for highly entangled polymers ($N = 250$) which has not been observed in previous work. The average entanglements per chain $\langle Z \rangle$ of the whole system in the block copolymer films are compared with homopolymer systems in Figure 3. The block copolymer possesses more entanglements than that of homopolymers under the same confined conditions due to the enhanced density of entanglements at the domain interface for the block copolymer systems. Finally, we note that there is almost no difference in $\langle Z \rangle$ between oriented lamellar films and fingerprint films.

3.2 Film Mechanics

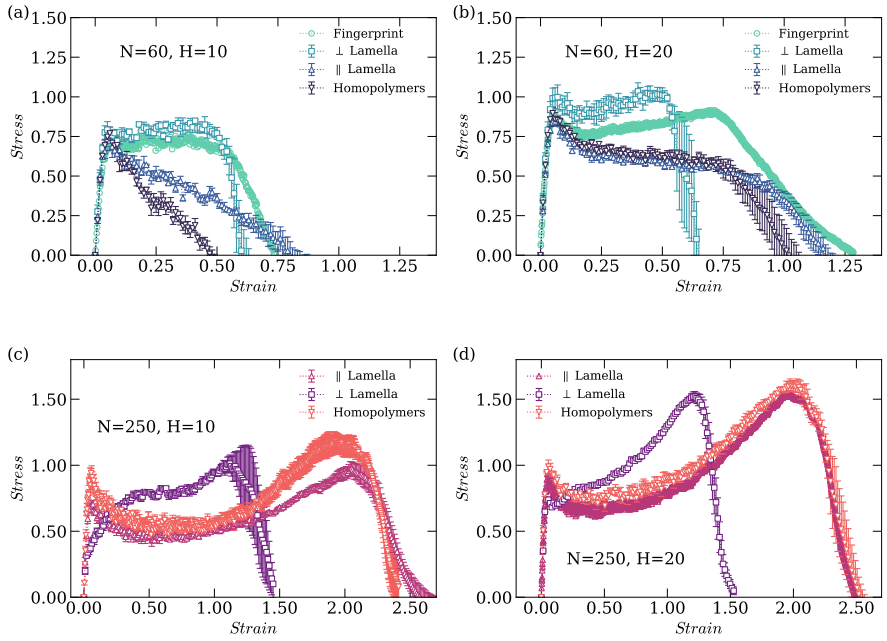

Figure 4. Stress-strain responses from the films with different thicknesses and different chain lengths N = 60 (a: H = 10σ, b: H = 20σ) and N = 250 (c: H = 10σ, d: H = 20σ). (⊥) denotes deformation along the direction perpendicular to the Lamella domains and (∥) parallel to the lamella domains.

We apply a constant-rate, uniaxial extension on the oriented lamellar films in the directions perpendicular and parallel to the plane of the lamellar interface, and in the stress-strain response calculation, we applied true strain to our system. As shown in Figure 4, for the short chain length systems with N=60, when deformed parallel to the interface the stress-strain responses are similar to the homopolymer films since there is no thickness variation in this direction, and visualization indicates that domain centers dominate the deformation mechanisms. On the other hand, when deformed perpendicular to the domains we find larger yield and plateau stresses, and in the two thicker films failure occurs at smaller strain than those in the homopolymer films. In the perpendicular deformation directions for those thick films, craze formation occurs at the center of the domains, and the film fails quickly due to the high concentration of chain ends in the center of

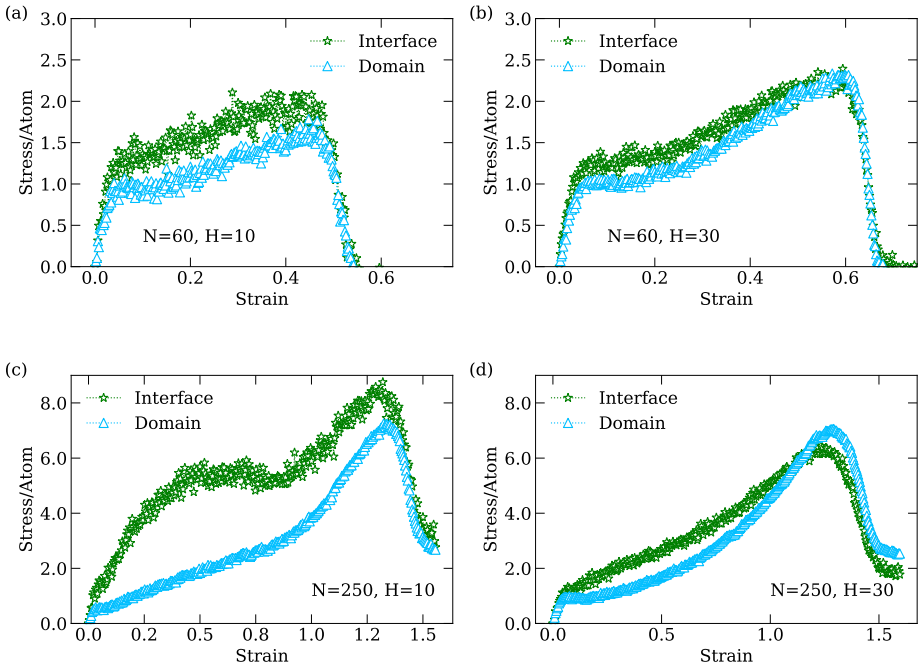

Figure 5. Stress per atom as a function of strain for domain boundary regions and domain center region in the systems of N=60 (H =10σ (a), H = 30σ (b)) and N=250 (H =10σ (c), H = 30σ (d)), when the deformation direction is perpendicular the domains.

the domain. In addition, the orientation of chains is more aligned in the oriented lamellar thin films than in the homopolymer system, which would facilitate chain pull-out in the block copolymer films. For the thinnest films, unlike the homopolymer, block copolymers still exhibit a strain plateau in their stress-strain responses, which is caused by the different strain localization mechanisms detailed below. In the entangled polymer systems N = 250, we observe very interesting behaviors in the $H = 10\sigma$ films where the stress-train response only exhibits a minimal glassy stiffness (the initial slope of the stress-strain curve) before transitioning to a much softer stress increase at small strains. In these films, the local film thickness is below 5σ near the domain boundaries, and the dynamics of particles in those regimes are more liquid-like due to the large portion of high mobility particles near free surfaces. Once the plastic rearrangement transitions

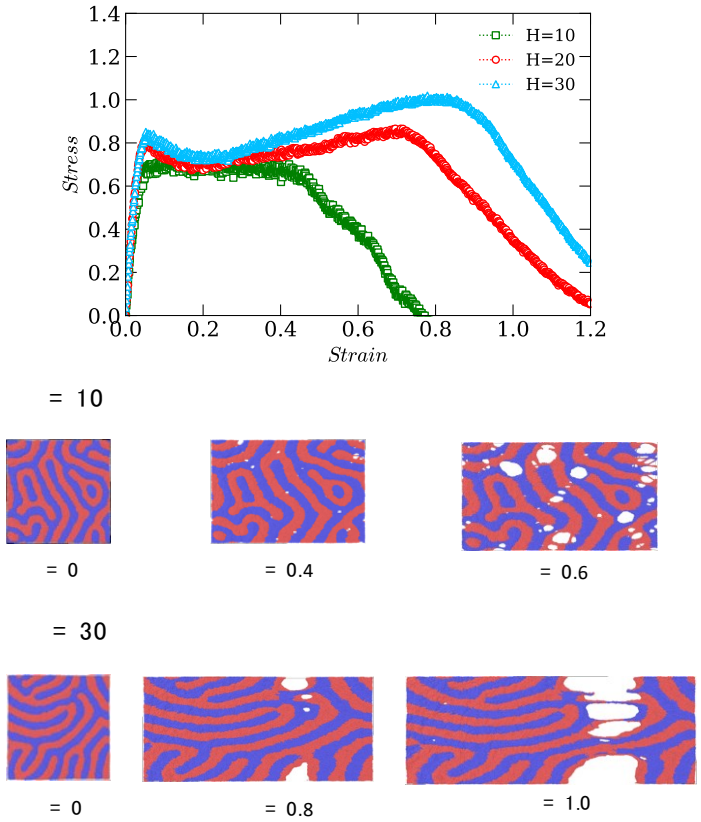

Figure 6. Comparison of stress-strain responses from film with fingerprint morphologies at different thicknesses with N = 60. The deformation morphologies at different strains are provided on the bottom.

into the center of domains, the typical strain plateau and strain hardening regimes of glassy entangled polymers start to show in the stress-strain curves. In the thicker films, the stress-strain response agrees with the behaviors of glassy homopolymers, where each regime of mechanical response is observed. Overall, compared to the homopolymers films, oriented lamellar thin films of highly entangled polymers exhibit smaller yield stress (the stress maximum immediately following the elastic response) and fail at much smaller strains when extended in the direction normal to the lamellae.

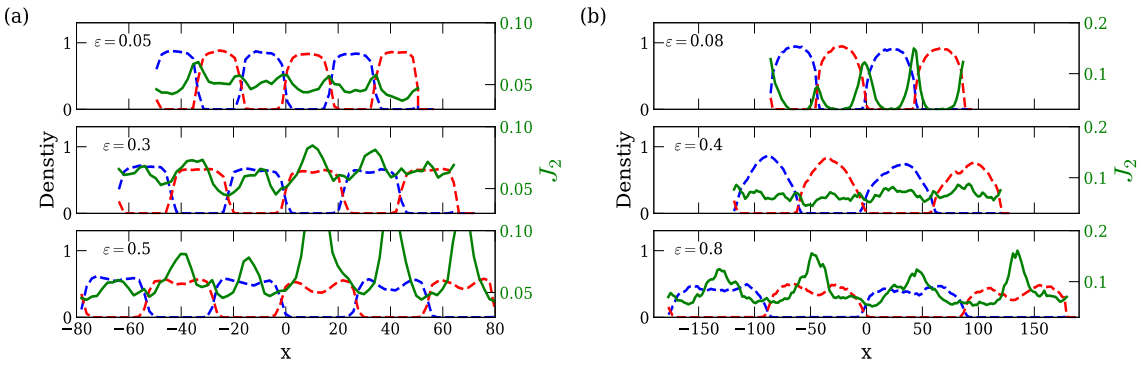

Figure 7. Deviatoric strain rate J_2 as a function of positions along x in the oriented lamellar films at selected strains for the systems with different chain lengths N = 60 (a) and N = 250 (b) at film thickness H = 20σ. The dash line (blue and red) is the density profiles across films.

In the oriented lamellar systems, the stress response is inhomogeneous across the lamellar domains when deforming along the direction perpendicular to the lamella in the $H = 10\sigma$ films. To calculate the local stress response, we define any monomer within 2σ of the A-B interface as part of the domain boundary, and the remaining monomers are defined as in the center of domains; our results are qualitatively insensitive to this choice. As shown in Figure 5, the monomers in the domain boundary region exhibit larger stresses than those in the domain center regions when the films thickness is 10σ, especially for the highly entangled systems N = 250, while the difference between those two regions is reduced for thicker films. The inhomogeneous stress distribution is mainly caused by the thickness perturbation in the films. The polymer chains deform faster around the domain boundaries and are stretched further than those in the domain center at the same strains. In the fingerprint films, the difference of stress per atom strain curve between domain boundary region and domain center region is reduced compared to the oriented films (see Supporting Figure S1).

Additionally, since defect-free block copolymer phases are much more challenging to fabricate experimentally, we performed the deformation process on the thin films with fingerprint

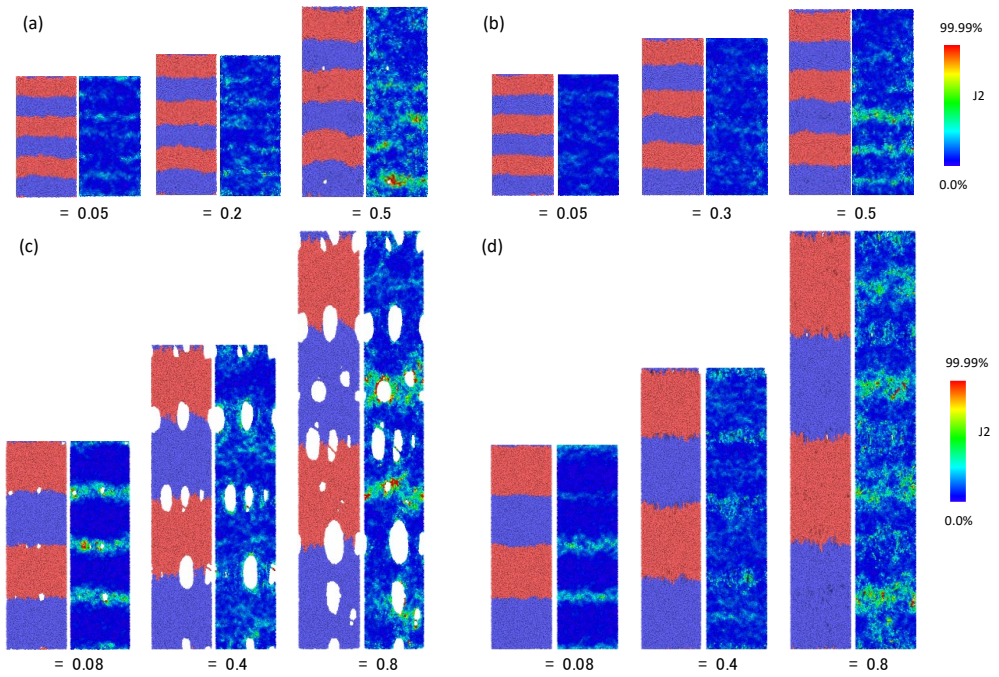

Figure 8. Snapshots of orientated lamellar films with different films thickness and different chain lengths N = 60 (a: $H = 10\sigma$ and b: $H = 20\sigma$), N = 250 (c: $H = 10\sigma$ and d: $H = 20\sigma$) at selected strains. The particles are color-coded by percentage of deviatoric strain rate J_2.

morphologies and compare their response with oriented lamellar films. As shown in Figure 6, for the short chain systems $N = 60$, the stress-strain responses have similar elastic behavior and yield stress as the oriented films, while the magnitude of plateau stresses is between oriented lamellar and homopolymer films. Fingerprint films begin to fail at larger strains than those of both oriented lamellar films and homopolymer films. Moreover, from the observation of the changes in the morphologies of the fingerprint films, we note that the strain localization is distributed across the films in the $H = 10\sigma$ films, and the voids tend to form in the areas near the domain boundaries. Small crazes are observed at nearly every void. However, for the thicker films $H = 30\sigma$, crazes are more localized in a single plane that spans the thickness of the film. The changes in the film

thicknesses affect the failure strain of the films but not the yield stresses, and stress plateaus are observed across all the film thicknesses.

To better understand the strain localization process in the block copolymer films, we collect particle configurations during deformation and extract the local strain rate associated with each particle (J_2), which is calculated for each monomer by performing the best-fit local affine transformation matrix[49], constructing the Lagrangian strain tensor, and extracting the deviatoric components of the strain tensor as $J_{2,i}(\varepsilon, \varepsilon + \Delta\varepsilon) = \frac{1}{\Delta\varepsilon}\sqrt{\frac{1}{3}Tr[\boldsymbol{\eta}_i - \eta_i^m \boldsymbol{I}]^2}$. Here $\boldsymbol{\eta}_i = \frac{1}{3}(\boldsymbol{J}_i^T \boldsymbol{J}_i - \boldsymbol{I})$ is the strain tensor for particle i, $\boldsymbol{J}_i$ is the best fit deformation gradient tensor[49] calculated based on the neighboring particles within distance of 2.5σ for particle i at strain ε over a lag strain $\Delta\varepsilon$, $\eta_i^m = \frac{1}{3}Tr[\boldsymbol{\eta}_i]$, and $\boldsymbol{I}$ is the identity matrix. Particles with large J_2 values have a higher deviatoric strain rate in their local environment and comparing J_2 across different locations in the film allows us to quantify where strain localization occurs. In the oriented lamellar films, we measure the J_2 based on the particle positions along the direction perpendicular to the domains at selected strains. As denoted by J_2 in Figure 7 and snapshots in Figure 8, we observe that the plastic rearrangements initially concentrate at the domain boundary between the two phases of the lamellae with craze

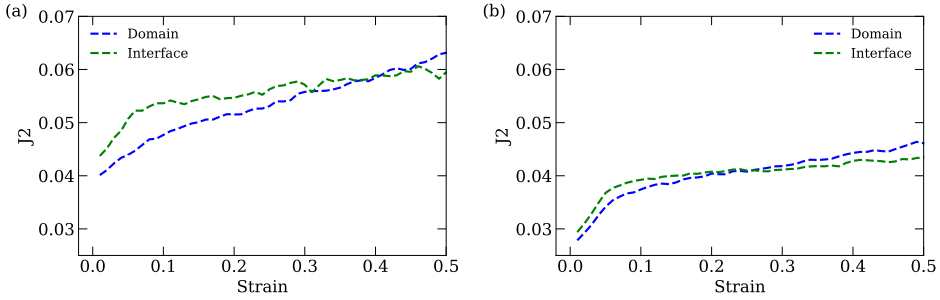

Figure 9. Average deviatoric strain rate J_2 as a function of strain based on the position of the particles (domain boundary or domain center) at different film thickness H = 10 (a) and H = 30 (b) in the films with fingerprint morphologies with N = 60.

formation at the onset of the deformation followed by craze widening. Next, strains translocate into the center of domains as the strains increase, resulting the stress in the stress-strain curve remaining at a high level. This phenomenon is most obvious in N = 250 and H=10σ systems. Once the strain localizes at the center area of the domains, the films break easily due to the high concentration of chain ends; this behavior is observed for all film thicknesses considered. Since the morphology of the fingerprint films is not as ordered as the oriented lamellar films, instead of calculating the particle positions, we divide the films into and domain boundary and the center of domain regions as we did in measuring the local stress response above. As shown in Figure 9, the plastic rearrangements in the domain boundaries are higher than that in the center of domains at small strains and become smaller in the large strains, which agrees with the findings in the oriented lamellar films. Even though near the domain boundaries the average entanglements per chain < Z > is larger than that of the other areas, the fast dynamics of the particles at the domain boundaries are presumed to be the primary cause of the initial strain localization.

To systematically compare mechanical behaviors across different systems, the toughness of each system, which describes the total amount of energy required to break the films, is calculated

by measuring the areas under stress strain curves, $\Gamma = \int_{\varepsilon=0}^{\varepsilon_{\sigma=0}} \sigma d\varepsilon$, where $\varepsilon_{\sigma=0}$ denotes the ε at which σ crosses zero. In our previous study, we found that toughness calculated from simulations follows a similar scaling as the strength of films measured in experiments as a function of the entanglement density.[16,50] In Figure 10, we compare the toughness of the oriented lamellar, fingerprint, and homopolymer films for N=60 at different film thicknesses. When the film thickness is equal to or larger than 20σ, fingerprint films are toughest among the geometries tested in this study, because they have more entanglements per chain than the homopolymers. The fact that fingerprint films

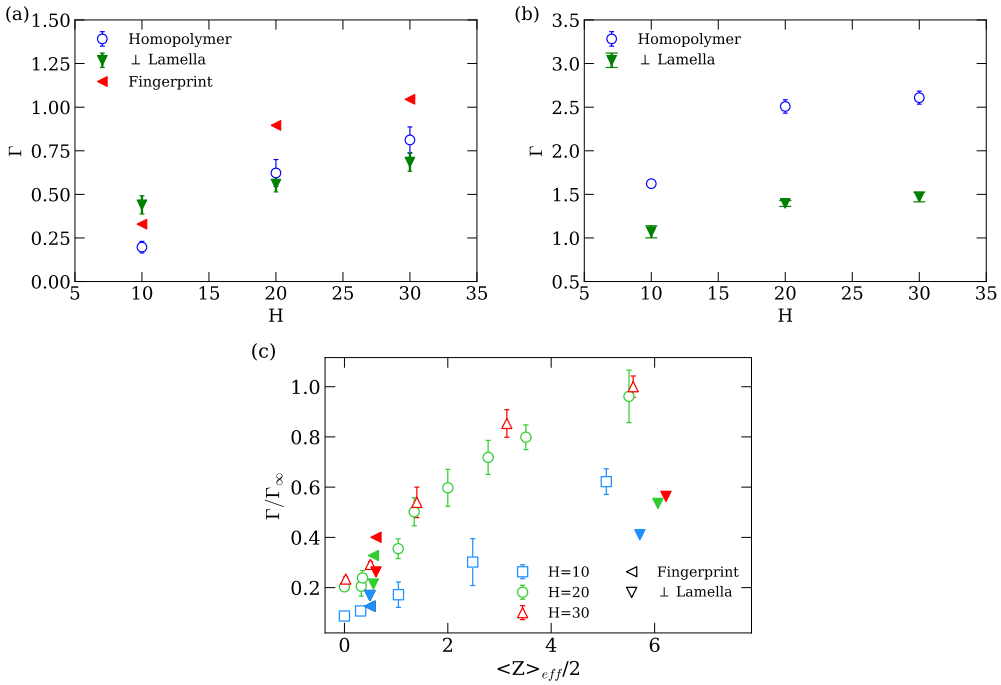

Figure 10. Toughness Γ as a function of the film thickness for polymers with chain length of N=60 (a) and N=250 (b) with different morphologies. (c) Normalized Toughness as a function of effective entanglements for both homopolymers and block copolymers. Γ_∞ is calculated from the homopolymer films with N = 250 and H = 30σ. For (c), hollow markers are toughness data of the blend homopolymer systems from our previous film thickness study[50] and solid markers are the toughness results from diblock copolymer films with all the chain lengths considered in this study. Each color corresponds to the film thickness H=10σ (blue), H=20σ (green), H=30σ (red), and the morphologies of diblock copolymer films is indicated by the shape of the markers. The top dashed line in (c) corresponds to the model proposed in our previous work,[16] and the bottom dashed line is a linear fit to the $H = 10\sigma$ data for the homopolymer films.

have disordered lamellar domains as oppose to ordered lamellar domains in the oriented lamellar films also contributes to the toughness. When the film thickness is 10σ, oriented lamellar films

are tougher than homopolymer films due to the prolonged plastic strain plateau in the stress-strain response.

In our previous work[50], we developed a model that describes the dependence of the toughness measured in simulations (or strength measured in experiments) on the number of effective entanglements per chain. In Figure 10c, the toughness of homopolymers and block copolymer films is compared against the model ($\frac{\Gamma}{\Gamma_\infty} = \left(1 - \frac{\Gamma_0}{\Gamma_\infty}\right) e^{\left(-\frac{2}{<Z_{eff}>}\right)} + \left(\frac{\Gamma_0}{\Gamma_\infty}\right)$, Γ_∞ is the toughness value of homopolymer systems $N = 250$ and $H = 30\sigma$, and Γ_0 is measured for chains of N = 10) as a function of effective entanglements. The toughness measured from the oriented lamellar films for the large N deviates significantly from the model proposed for the homopolymers.[16] We hypothesize this is due not only to the inhomogeneous entanglement distributions but also the alignments of domain boundaries affect the mechanical properties of the films. For fingerprint block copolymers with the chain lengths simulated here track the model, though the number of data points is limited.

In the block copolymer systems, the interactions χ between different components play an important role in determining the phase separations and morphologies, we investigate the stress-strain curves for fingerprint systems with different χ in the supporting materials (see Supporting Figure S2); we do not observe a significant difference between those two systems, which suggests that small changes in the ε_{AB} do not significantly affect the mechanical response of the glassy block copolymer systems.

4 Conclusion

In summary, we investigate the role of morphology, specifically orientation, and confinement on the segmental dynamics and inter-chain entanglements with regards to mechanical response of

glassy lamellar diblock copolymer polymer films under uniaxial tension using molecular dynamics simulations. By analyzing the thickness profiles of the block copolymer thin films, we notice that there are very large film thickness perturbations across the thin films, which in turn affects the local segmental dynamics of the films, due to the strong segregation between each type of domains. Notably, the perturbations in the film thickness with longer chains is stronger compared to the short chain systems. In addition, in the portions of the chain that are close to the domain boundaries, there is an increase in the number of entanglements, which makes the overall average entanglement per chain in the block copolymer systems larger than that of the homopolymer systems at the same chain length. From the mechanical responses of block copolymers films with short chains N = 60, the behaviors of films with fingerprint morphologies are more ductile compared to the oriented lamellar films and homopolymers and the toughness is also larger, due to the increase in the randomness of the domain orientation and entanglements per chain. Oriented lamellar films have the smallest toughness compared to fingerprint and homopolymers since failure tends to occur near the center of the block copolymer domains due to the high concentration of chain ends that are unable to support stress. Furthermore, during the deformation in the block copolymers films, the plastic rearrangements initially concentrate at the boundary between the two phases of the lamellae until close to failure, when the plasticity moves to the center of a domain. Our findings of the glassy block copolymer thin film mechanics provide molecular insight into how segmental mobility and entanglements interplay with position and morphology to control the mechanics of thin polymer films and design of mechanically-robust polymer thin films.

ASSOCIATED CONTENT

Supporting Information.

Supporting stress-strain per atom responses of block thin films with fingerprint morphologies, and stress-strain responses with different interactions ε_{AB} between type A and B monomers (PDF).

AUTHOR INFORMATION

Corresponding Author

*E-mail rrig@seas.upenn.edu (R.A.R.).

Author Contributions

The manuscript was written through contributions of all authors. All authors have given approval to the final version of the manuscript.

Funding Sources

Z.T., and R.A.R. acknowledge support from NSF DMR 1904776. This research used the Extreme Science and Engineering Discovery Environment (XSEDE), which is supported by NSF ACI-1548562, accessed through allocation TG-DMR 150034. The authors also thank Alfred J. Crosby, and Cynthia Bukowski for helpful discussions.

(1) Keddie, J. L.; Jones, R. A. L.; Cory, R. A. Size-Dependent Depression of the Glass Transition Temperature in Polymer Films. *Europhys. Lett.* **1994**, *27* (1), 59–64.
(2) Stafford, C. M.; Harrison, C.; Beers, K. L.; Karim, A.; Amis, E. J.; VanLandingham, M. R.; Kim, H.-C.; Volksen, W.; Miller, R. D.; Simonyi, E. E. A Buckling-Based Metrology for Measuring the Elastic Moduli of Polymeric Thin Films. *Nat. Mater.* **2004**, *3* (8), 545–550.
(3) Liu, Y.; Chen, Y. C.; Hutchens, S.; Lawrence, J.; Emrick, T.; Crosby, A. J. Directly Measuring the Complete Stress-Strain Response of Ultrathin Polymer Films. *Macromolecules* **2015**, *48* (18), 6534–6540.
(4) Bay, R. K.; Shimomura, S.; Liu, Y.; Ilton, M.; Crosby, A. J. Confinement Effect on Strain Localizations in Glassy Polymer Films. *Macromolecules* **2018**, *51* (10), 3647–3653.
(5) Bay, R. K.; Crosby, A. J. Uniaxial Extension of Ultrathin Freestanding Polymer Films. *ACS Macro Lett.* **2019**, *8* (9), 1080–1085.

(6) Riggleman, R. A.; Lee, H. N.; Ediger, M. D.; De Pablo, J. J. Heterogeneous Dynamics during Deformation of a Polymer Glass. *Soft Matter* **2010**, *6* (2), 287–291.
(7) Shavit, A.; Riggleman, R. A. Physical Aging, the Local Dynamics of Glass-Forming Polymers under Nanoscale Confinement. *J. Phys. Chem. B* **2014**, *118* (30), 9096–9103.
(8) Yang, F.; Ghosh, S.; Lee, L. J. Molecular Dynamics Simulation Based Size and Rate Dependent Constitutive Model of Polystyrene Thin Films. *Comput. Mech.* **2012**, *50* (2), 169–184.
(9) Van Workum, K.; De Pablo, J. J. Computer Simulation of the Mechanical Properties of Amorphous Polymer Nanostructures. *Nano Lett.* **2003**, *3* (10), 1405–1410.
(10) Yoshimoto, K.; Jain, T. S.; Nealey, P. F.; De Pablo, J. J. Local Dynamic Mechanical Properties in Model Free-Standing Polymer Thin Films. *J. Chem. Phys.* **2005**, *122* (14).
(11) Xia, W.; Lan, T. Interfacial Dynamics Governs the Mechanical Properties of Glassy Polymer Thin Films. *Macromolecules* **2019**, *52* (17), 6547–6554.
(12) Ge, T.; Tzoumanekas, C.; Anogiannakis, S. D.; Hoy, R. S.; Robbins, M. O. Entanglements in Glassy Polymer Crazing: Cross-Links or Tubes? *Macromolecules* **2017**, *50* (1), 459–471.
(13) Bay, R. K.; Zhang, T.; Shimomura, S.; Ilton, M.; Tanaka, K.; Riggleman, R. A.; Crosby, A. J. Decoupling the Impact of Entanglements and Mobility on the Failure Properties of Ultrathin Polymer Films. *Macromolecules* **2022**.
(14) Wang, B.; Luo, D.; Li, Z.; Kwon, Y.; Wang, M.; Goo, M.; Jin, S.; Huang, M.; Shen, Y.; Shi, H.; et al. Camphor-Enabled Transfer and Mechanical Testing of Centimeter-Scale Ultrathin Films. *Adv. Mater.* **2018**, *30* (28), 1–8.
(15) Galuska, L. A.; Muckley, E. S.; Cao, Z.; Ehlenberg, D. F.; Qian, Z.; Zhang, S.; Rondeau-Gagné, S.; Phan, M. D.; Ankner, J. F.; Ivanov, I. N.; et al. SMART Transfer Method to Directly Compare the Mechanical Response of Water-Supported and Free-Standing Ultrathin Polymeric Films. *Nat. Commun.* **2021**, *12* (1), 2347.
(16) Bukowski, C.; Zhang, T.; Riggleman, R. A.; Crosby, A. J. Load-Bearing Entanglements in Polymer Glasses. *Sci. Adv.* **2021**, *7* (38), 1–10.
(17) Schwier, C. E.; Argon, A. S.; Cohen, R. E. Crazing in Polystyrene-Polybutadiene Diblock Copolymers Containing Cylindrical Polybutadiene Domains. *Polymer (Guildf).* **1985**, *26* (13), 1985–1993.
(18) Schwier, C. E.; Argon, A. S.; Cohen, R. E.; Schwier, C. E. Craze Plasticity in a Series of Polystyrene/Polybutadiene Di-Block Copolymers with Spherical Morphology. *Philos. Mag. A Phys. Condens. Matter, Struct. Defects Mech. Prop.* **1985**, *52* (5), 581–603.
(19) Honeker, C. C.; Thomas, E. L. Impact of Morphological Orientation in Determining Mechanical Properties in Triblock Copolymer Systems. *Chem. Mater.* **1996**, *8* (8), 1702–1714.
(20) Weidisch, R.; Ensslen, M.; Michler, G. H.; Fischer, H. Deformation Behavior of Weakly Segregated Block Copolymers. 1. Influence of Morphology of Poly(Styrene-6-Butyl Methacrylate) Diblock Copolymers. *Macromolecules* **1999**, *32* (16), 5375–5382.
(21) Weidisch, R.; Ensslen, M.; Michler, G. H.; Arnold, M.; Budde, H.; Höring, S.; Fischer, H. A Novel Scheme for Prediction of Deformation Mechanisms of Block Copolymers Based on Phase Behavior. *Macromolecules* **2001**, *34* (8), 2528–2535.
(22) Fujimura, M.; Hashimoto, T.; Kawai, H. Structural Change Accompanied by Plastic-to-Rubber Transition of SBS Block Copolymers. *Rubber Chem. Technol.* **1978**, *51* (2), 215–224.

(23) Uno, H.; Hashimoto, T.; Fujimura, M. Microdomain Structure and Some Related Properties of Block Copolymers. II. Plastic Deformation Mechanisms of the Glassy Component in Rubber-Toughened Plastics. *J. Macromol. Sci. Part B* **1980**, *17* (3), 427–472.
(24) Cohen, Y.; Albalak, R. J.; Dair, B. J.; Capel, M. S.; Thomas, E. L. Deformation of Oriented Lamellar Block Copolymer Films. *Macromolecules* **2000**, *33* (17), 6502–6516.
(25) Makke, A.; Lame, O.; Perez, M.; Barrat, J. L. Influence of Tie and Loop Molecules on the Mechanical Properties of Lamellar Block Copolymers. *Macromolecules* **2012**, *45* (20), 8445–8452.
(26) Makke, A.; Perez, M.; Lame, O.; Barrat, J. L. Nanoscale Buckling Deformation in Layered Copolymer Materials. *Proc. Natl. Acad. Sci. U. S. A.* **2012**, *109* (3), 680–685.
(27) Lee, J. Y.; Crosby, A. J. Crazing in Glassy Block Copolymer Thin Films. *Macromolecules* **2005**, *38* (23), 9711–9717.
(28) Ryu, C. Y.; Ruokolainen, J.; Fredrickson, G. H.; Kramer, E. J.; Hahn, S. F. Chain Architecture Effects on Deformation and Fracture of Block Copolymers with Unentangled Matrices. *Macromolecules* **2002**, *35* (6), 2157–2166.
(29) Shi, A. C.; Li, B. Self-Assembly of Diblock Copolymers under Confinement. *Soft Matter* **2013**, *9* (5), 1398–1413.
(30) Yu, B.; Sun, P.; Chen, T.; Jin, Q.; Ding, D.; Li, B.; Shi, A. C. Confinement-Induced Novel Morphologies of Block Copolymers. *Phys. Rev. Lett.* **2006**, *96* (13), 1–4.
(31) Detcheverry, F. A.; Kang, H.; Daoulas, K. C.; Müller, M.; Nealey, P. F.; De Pablo, J. J. Monte Carlo Simulations of a Coarse Grain Model for Block Copolymers and Nanocomposites. *Macromolecules* **2008**, *41* (13), 4989–5001.
(32) Detcheverry, F. A.; Pike, D. Q.; Nealey, P. F.; Müller, M.; de Pablo, J. J. Simulations of Theoretically Informed Coarse Grain Models of Polymeric Systems. *Faraday Discuss.* **2010**, *144*, 111–125.
(33) Detcheverry, F. A.; Pike, D. Q.; Nagpal, U.; Nealey, P. F.; de Pablo, J. J. Theoretically Informed Coarse Grain Simulations of Block Copolymer Melts: Method and Applications. *Soft Matter* **2009**, *5* (24), 4858.
(34) Sethuraman, V.; Kipp, D.; Ganesan, V. Entanglements in Lamellar Phases of Diblock Copolymers. *Macromolecules* **2015**, *48* (17), 6321–6328.
(35) Kremer, K.; Grest, G. S. Erratum: Dynamics of Entangled Polymer Melts: A Molecular-dynamics Simulation [J. Chem. Phys. 9 2 , 5057 (1990)]. *J. Chem. Phys.* **1991**, *94* (5), 4103–4103.
(36) Kumar, R.; Goswami, M.; Sumpter, B. G.; Novikov, V. N.; Sokolov, A. P. Effects of Backbone Rigidity on the Local Structure and Dynamics in Polymer Melts and Glasses. *Phys. Chem. Chem. Phys.* **2013**, *15* (13), 4604–4609.
(37) Sides, S. W.; Grest, G. S.; Stevens, M. J.; Plimpton, S. J. Effect of End-Tethered Polymers on Surface Adhesion of Glassy Polymers. *J. Polym. Sci. Part B Polym. Phys.* **2004**, *42* (2), 199–208.
(38) Mavrantzas, V. G.; Boone, T. D.; Zervopoulou, E.; Theodorou, D. N. End-Bridging Monte Carlo: A Fast Algorithm for Atomistic Simulation of Condensed Phases of Long Polymer Chains. *Macromolecules* **1999**, *32* (15), 5072–5096.
(39) Banaszak, B. J.; De Pablo, J. J. A New Double-Rebridging Technique for Linear Polyethylene. *J. Chem. Phys.* **2003**, *119* (4), 2456–2462.
(40) Auhl, R.; Everaers, R.; Grest, G. S.; Kremer, K.; Plimpton, S. J. Equilibration of Long

Chain Polymer Melts in Computer Simulations. *J. Chem. Phys.* **2003**, *119* (24), 12718–12728.
(41) Plimpton, S. Fast Parallel Algorithms for Short-Range Molecular Dynamics. *J. Comput. Phys.* **1995**, *117* (1), 1–19.
(42) Thompson, A. P.; Aktulga, H. M.; Berger, R.; Bolintineanu, D. S.; Brown, W. M.; Crozier, P. S.; in 't Veld, P. J.; Kohlmeyer, A.; Moore, S. G.; Nguyen, T. D.; et al. LAMMPS - a Flexible Simulation Tool for Particle-Based Materials Modeling at the Atomic, Meso, and Continuum Scales. *Comput. Phys. Commun.* **2022**, *271*, 108171.
(43) Baglay, R. R.; Roth, C. B. Local Glass Transition Temperature Tg(z) of Polystyrene next to Different Polymers: Hard vs. Soft Confinement. *J. Chem. Phys.* **2017**, *146* (20).
(44) Lang, R. J.; Merling, W. L.; Simmons, D. S. Combined Dependence of Nanoconfined T g on Interfacial Energy and Softness of Confinement. *ACS Macro Lett.* **2014**, *3* (8), 758–762.
(45) Kröger, M. Shortest Multiple Disconnected Path for the Analysis of Entanglements in Two- and Three-Dimensional Polymeric Systems. *Comput. Phys. Commun.* **2005**, *168* (3), 209–232.
(46) Shanbhag, S.; Kröger, M. Primitive Path Networks Generated by Annealing and Geometrical Methods: Insights into Differences. *Macromolecules* **2007**, *40* (8), 2897–2903.
(47) Ramírez-Hernández, A.; Peters, B. L.; Schneider, L.; Andreev, M.; Schieber, J. D.; Müller, M.; Kröger, M.; De Pablo, J. J. A Detailed Examination of the Topological Constraints of Lamellae-Forming Block Copolymers. *Macromolecules* **2018**, *51* (5), 2110–2124.
(48) Alshammasi, M. S.; Escobedo, F. A. Correlation between Morphology and Anisotropic Transport Properties of Diblock Copolymers Melts. *Soft Matter* **2019**, *15* (5), 851–859.
(49) Falk, M. L.; Langer, J. S. Dynamics of Viscoplastic Deformation in Amorphous Solids. *Phys. Rev. E* **1998**, *57* (6), 7192–7205.
(50) Zhang, T.; Riggleman, R. A. Thickness-Dependent Mechanical Failure in Thin Films of Glassy Polymer Bidisperse Blends. *Macromolecules* **2022**, *55* (1), 201–209.